AIAA JOURNAL
Vol. 33, No. 3, March 1995

Interferometric Study of Organized Motions in Turbulent Boundary Layers

S. Zhong* and L. C. Squire†
University of Cambridge, Cambridge CB2 1PZ, England, United Kingdom

Double-pulse holographic interferometry has been used to visualize organized structures in zero-pressure-gradient turbulent boundary layers over a flat plate at $M = 1.8$, 2.5, and 3.6 ($Re_\theta = 1.2 \times 10^4$ to 2.2×10^4). Differential interferograms taken with a pulse interval between 2 to 600 μs at three different Mach numbers show an interesting array of fringe cells that appear inclined downstream in the boundary layers. These fringe cells must be the interferometric images of large-scale outer-layer structures convecting in the main flow direction. On absolute interferograms of the boundary layers, the interferometric images appear as horizontal fringe lines running over the test surface. The wavy fringe pattern frequently exhibits distinct inclined interfaces with a positive upstream density gradient that must be associated with the backs of large-scale outer-layer bulges. Quantitative information of these structures has been extracted from the interferograms that is in agreement with data from other investigators using different experimental techniques. To aid the interpretation of the experimental data, interferograms have been generated numerically with the database from a large-eddy simulation. These interferograms also reveal regular fringe patterns in the boundary layer that are found to be produced by the large-scale structures in the layer.

Nomenclature

H = boundary-layer shape factor, δ^*/θ
L = width of tunnel test section, 114×10^{-3} m
M = freestream Mach number
N = order number of fringes
Re_θ = Reynolds number based on momentum thickness θ
u_∞ = freestream velocity
Δt = laser pulse interval, μs
δ = boundary-layer thickness, mm
δ^* = boundary-layer displacement, mm
κ = Dale–Gladstone constant, 2.24×10^{-4} m^3/kg
λ = wavelength of laser light, 694×10^{-9} m

Introduction

ORGANIZED structures are found to exist in turbulent shear flows and are responsible for turbulence production and transportation.[1–4] A better understanding of the dynamics of these structures is the key to the improvement of turbulence modeling and the implementation of effective turbulence control. Organized structures in turbulent boundary layers have been well studied for decades. However, most of the studies were conducted in low-speed flows since simplicity of the experimental setup and the physically large sublayer regions ease research. Stimulated by a renewed interest in high-speed aircraft, a series of experiments have been carried out on turbulent boundary layers at freestream Mach numbers up to 2.9 in Princeton University in the late 1980s. Hot-wire, schlieren and Rayleigh scattering techniques were employed to capture the traces of organized structures in the flow,[5,6] and these studies have yielded interesting results. It is felt, however, that a similar study with a different approach, i.e., holographic interferometry, might add to our knowledge of these structures. Holographic interferometry relies on a changing density or reflective index to provide a nonintrusive instantaneous whole field visualization of the flow. It is an attractive technique to study turbulence in compressible flows due to its high resolution to density changes, the possibility of visualizing organized structures at different scales andin a three-dimensional manner.

One of the difficulties with the present analysis is in the actual interpretation of the various types of fringe pattern, particularly in the differential interferograms. To aid this interpretation a large-eddy simulation database was postprocessed to produce absolute and differential interferograms. Although the database used was for incompressible flow at a much lower Reynolds number than that of the experiments, the computed fringes showed some similarities to those observed in the experimental fringes. Thus by interrogation of the database it should be possible to relate particular fringe patterns to actual flow structures. Since the physical conditions in our experiments are so different from those used in the large-eddy simulation, these comparisons must be treated with caution, and only a brief account of the results from this analysis is given here.

Experimental Studies

Principles of Holographic Interferometry

In double-pulse interferometry, two exposures are required to be taken through the flowfield of interest. Two basic techniques are usually employed: 1) an absolute interferogram is produced by taking the first exposure without the flow, the second in the presence of the flow; 2) a differential interferogram is made by taking two exposures in rapid succession with the flow on. Simultaneous reconstruction of the two holographic recordings produces a wave pattern that is the superposition of the light wavefronts in the two separate exposures. The interference fringes, seen by viewing the reconstructed images, are related to the density field of the flow at the two instants of exposure by[7]

$$N\lambda = \int_0^L \kappa[\rho(x, y, z, t + \Delta t) - \rho(x, y, z, t)]\,\mathrm{d}z \qquad (1)$$

For strictly two-dimensional flows Eq. (1) reduces to $N\lambda = \kappa \Delta\rho L$ from which it is deduced that the density difference $\Delta\rho$ between two consecutive dark or bright fringes is 0.027 Kg/m^3 for the present experiments. Consequently, the density distribution across a two-dimensional boundary layer can be obtained by counting fringes from known conditions in the freestream. The ruby laser produces pulses with a duration of 30 ns, which is two orders of magnitude smaller than the convection time scale of large eddies in the boundary layers. Therefore an absolute interferogram can be regarded

Received April 2, 1994; presented as Paper 94-2233 at the AIAA 25th Fluid Dynamics, Plasmadynamics, and Lasers Conference, Colorado Springs, CO, June 20–23, 1994; revision received Nov. 22, 1994; accepted for publication Nov. 28, 1994.

*Currently Research Assistant at Department of Engineering Science, University of Oxford, Oxford OX1 3PJ, England, United Kingdom. Student Member AIAA.

†Reader, Department of Engineering. Associate Fellow AIAA.

as an instantaneous visualization of the flow, whereas a differential interferogram can be regarded as a record of time evolution of turbulence structures during a given time interval. Other technical details of the optical system used can be found in Ref. 8.

Test Conditions

All of the results presented here were obtained from boundary layers developed on a flat surface placed along the centerline of the intermittent supersonic tunnel in the Cambridge University Engineering Department. The boundary layers develop under zero-pressure-gradient and adiabatic conditions over about 0.45 m before reaching the test region in the center of the viewing windows of 203-mm diameter. The test section has a cross-sectional area of 83 mm (height) × 114 mm (width) at this position. Two-dimensionality of the boundary-layer flows has been checked in terms of surface oil flow patterns and total pressure distributions across the span in earlier investigations.[9–11] At Mach numbers up to 2.5, it has been found that the flow is parallel and that the profiles are similar across the center 80% of the tunnel span; also, in this speed range the measured profiles and skin-friction coefficients satisfy the two-dimensional momentum equation. This good two-dimensionality is confirmed by the excellent agreement found between density profiles measured on the centerline and profiles deduced from the interference fringes that result from an integration of the density field across the span. There is more evidence of three-dimensionality at $M = 3.6$ where the flow in the corners shows signs of streamwise vortices and where errors of up to 10% have been observed in two-dimensional checks. The departure from two-dimensionality at this Mach number is borne in mind in the following discussion of results. The full test conditions measured with a pitot probe at the midspan are given in Table 1 with uncertainties in the measured flow variables listed in the last column. Two different Reynolds numbers have been tested at $M = 1.8$ and 2.5.

Absolute Interferograms

In the absolute interferograms for two-dimensional zero-pressure-gradient boundary layers, fringe lines with variable spacings run almost parallel to the test surface, and these fringes represent lines of constant density. With a close look at the boundary layer, one sees that the fringes appear very ragged (Fig. 1a). The raggedness penetrates almost the entire boundary layer and appears in waves inclined downstream. These wavy structures must be related to the turbulence. In particular, strong upstream density gradients or interfaces are often seen to occur upstream of a region with fringes spreading upwards where the density is smaller relative to its neighboring region (see arrow in Fig. 1a). This type of fringe pattern is frequently seen on absolute interferograms of turbulent boundary layers and indicates that some distinct events occur along the spanwise direction of the layer.

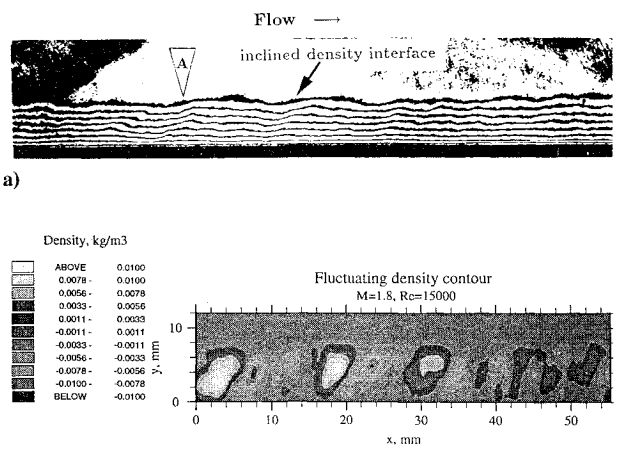

Fig. 1 a) Absolute interferogram and b) contours of fluctuating density deduced from interferograms ($M = 1.8$, and $Re_\theta = 1.5 \times 10^4$).

To get an insight into the features responsible for the wavy fringe pattern observed, quantitative density information of the boundary layer is required. The interferograms were first image processed to obtain the coordinates of fringe lines. The density at an intermediate point between two consecutive fringes was deduced by linear interpolation of known density on the two fringes. Note, due to the presence of a large positive density gradient very close to wall, the light rays tend to bend away from the surface and this leads to lost of fringes (usually one to three fringes for the present tests) in this region. However, this effect is found to be confined within 0.2δ and does not affect the information extracted on the outer-layer structures. Density fluctuations were then obtained by subtracting mean from instantaneous values. A mean density profile can be obtained from the interferogram by spatial averaging the instantaneous density at a constant height from the test surface along the whole length of the boundary layer (about 65 mm). The mean density profiles obtained thereby have been compared with those measured by a pitot probe. The agreement between mean density profiles by two different methods is good at Mach numbers up to 2.5, again confirming the good two-dimensionality of the flow. At $M = 3.6$, however, the discrepancy is about 10% at $y/\delta = 0.5$. This is because the interferometry integrates across the layer so that the nonuniformity in the flow makes the density profile from interferograms depart from that measured at the midspan. Considering this factor, it was decided to use the spatial-averaged density profiles deduced from the interferograms instead of those from pitot measurements as the mean so that the integrated effect on the density fluctuations can be canceled out. The density fluctuations obtained from the interferograms are, of course, much smaller than those measured at a single point since the turbulence is associated with highly localized features across the span. This analysis, however, does produce some useful information about the turbulent structures.

On the contour maps of fluctuating density (Fig. 1b), cells of density deficit and excess relative to the surroundings are found arranged in an alternating manner in the boundary layer. They appear inclined downstream at about 60 deg to the wall and have a vertical and streamwise dimension comparable to the boundary-layer thickness. The cells of density deficit are recognized as the images of large-scale turbulent bulges that are formed from lumps of warm air ejected from the near wall-region. The dimension and orientation of these cells are in agreement with the observations made by other investigators with different experimental techniques.[5,6] Sharp density interfaces appear where the warm air inside the bulge and the cool air outside meet. It is these density interfaces that are responsible for the fingerlike blobs detected by the schlieren technique, which is sensitive to the first derivative of the density.[5] The fact that the positive upstream density gradient is usually sharper than the negative ones is because the higher density nonturbulent fluid moves slightly faster than the lower density bulges and pushes them from behind. The similarity of density fluctuations around the inclined interface with a positive upstream density gradient (see Fig. 2) to the hot-wire signal $(\rho u)'$ detected as a positive VITA event (Fig. 15 in Ref. 12) should also be noticed. Considering that the density fluctuations are

Table 1 Test conditions

M	1.8	1.8	2.5	2.5	3.6	±0.03
ρ_e, kg/m^3	0.60	0.79	0.42	0.77	0.44	±0.01
ρ_w, kg/m^3	0.36	0.48	0.19	0.35	0.12	±0.01
δ, mm	5.8	5.8	6.5	6.1	6.7	±0.1
θ, mm	0.49	0.48	0.51	0.46	0.40	±0.02
H	2.73	2.71	4.08	3.96	6.90	—
Re_θ	1.2×10^4	1.5×10^4	1.4×10^4	2.2×10^4	2.0×10^4	—

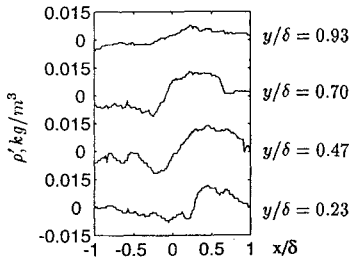

Fig. 2 Density fluctuations around the inclined interface in region A marked in Fig. 1a. Note, in order to be compared with Fig. 15 in Ref. 12, here $+x$ is in the upstream direction.

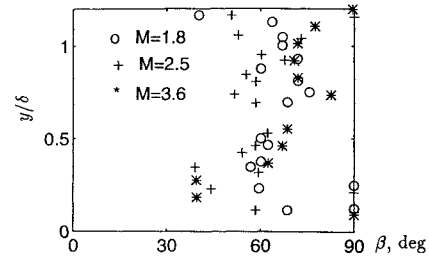

Fig. 3 Inclined angle of density interfaces deduced from absolute interferograms.

correlated with the mass-flux fluctuations, the inclined density interface and positive VITA event must be associated with the same sort of features, i.e., the backs of turbulent outer-layer bulges.

As a distinct pattern in the flow, the structure angle of the inclined interface can be examined statistically by means of spatial correlation of density fluctuations. The correlation of the density fluctuations at various heights ($y = y_0 + \eta$) with those at a reference vertical station y_0 can be obtained with the following expression:

$$\Re_{12}(x_0, y_0, \xi, \eta) = \frac{\overline{\rho_1'(x_0, y_0)\rho_2'(x_0 + \xi, y_0 + \eta)}}{\left(\overline{\rho_1'^2}\,\overline{\rho_2'^2}\right)^{\frac{1}{2}}} \qquad (2)$$

where ξ and η are a multiple of a mesh grid division in the streamwise (x) and the vertical (y) direction, respectively. The calculation yields an angle between a segment of the interface and the wall,

$$\beta(y_0, \eta) = \arctan\left(\frac{\eta}{\xi_1}\right) \qquad (3)$$

Here ξ_1 is ξ where a maximum correlation is reached for a particular y_0 ($= 0.6\delta$ here) and η.

The mean structure angle at the three Mach numbers ranges from 40 to 75 deg for $0.2 < y/\delta < 1.0$ with the smaller angle occurring in the inner half of the boundary layer (see Fig. 3). (The angle of 90 deg for $y < 0.2$ is caused by low spatial resolution of density fluctuations in that region.) At $y/\delta = 0.8$, the angle is between 55 and 75 deg. It is in agreement within data scatter with that obtained by Spina et al.[6] with hot wires ($\beta = 48$–72 deg at $M = 2.9$) and Smith[5] with schlieren technique ($\beta = 65$ deg at $M = 2.45$). No obvious trend of changes in β with Reynolds number and Mach number was observed.

Differential Interferograms

A typical set of differential interferograms are shown in Fig. 4 for the higher Reynolds number tested at $M = 2.5$. These interferograms present an interesting array of fringe cells in the flow. The cells occur in a relatively regular way along the whole length of the boundary layer suggesting that a mechanism exists for their regular production.

The most frequently repeated image pattern is a striation with a bright center surrounded by a single black ring or two concentric black rings (Figs. 4b and 4d). Since interference fringes are contours of phase difference, such an interferometric pattern indicates a gradient of optical phase change, most likely a gradient of density

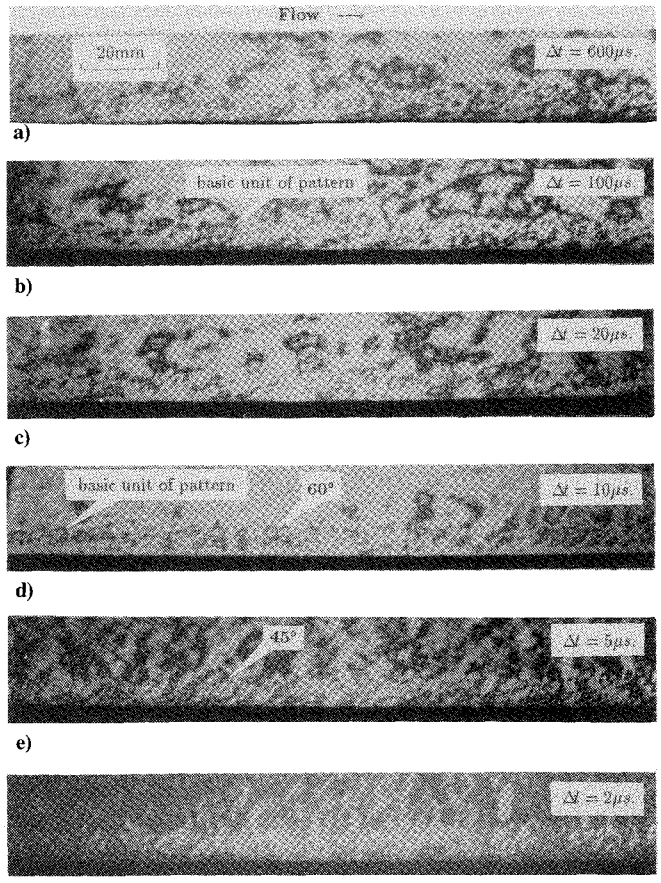

Fig. 4 Differential interferograms, $M = 2.5$ and $Re_\theta = 2.2 \times 10^4$.

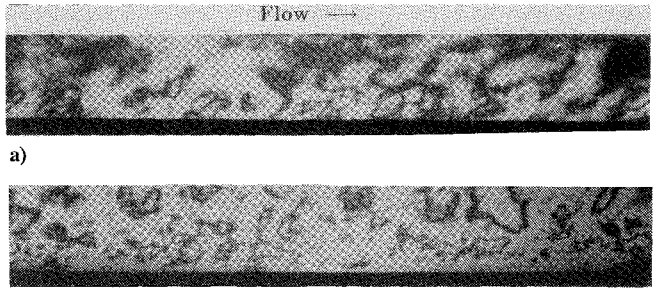

Fig. 5 Differential interferograms: a) $M = 2.5$, $Re_\theta = 1.4 \times 10^4$, and $\Delta t = 100$ μs; and b) $M = 3.6$, $Re_\theta = 2.0 \times 10^4$, and $\Delta t = 60$ μs.

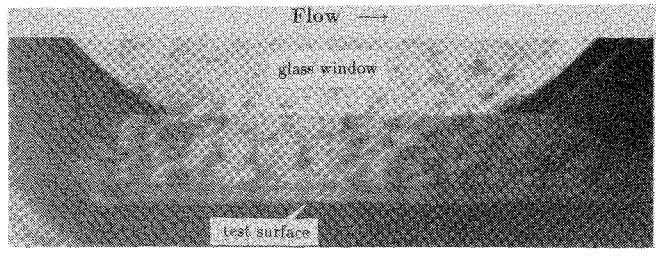

Fig. 6 Differential interferogram obtained by focusing the camera on the test surface, $M = 1.8$, $Re_\theta = 1.5 \times 10^4$, and $\Delta t = 10$ μs.

change in the radial direction over the spatial extent of the fringe cell. This kind of fringe pattern must be produced by convection of the large-scale flow features revealed by the contour map of fluctuating density (Fig. 2) in the main flow direction.

Since it is the displacement of the flow feature that determines the optical phase shift, it follows that the time interval Δt_c required for an organized structure to move downstream by a distance equal to its streamwise dimension is the critical time interval for the change of pattern with pulse intervals. If the streamwise dimension of turbulent

eddies is assumed to be one boundary-layer thickness and the convection velocity to be $0.9u_\infty$ based on the hot-wire measurement by Spina et al.,[6] the pulse interval Δt_c is then approximately $1.1\delta/u_\infty$ or 12 μs for $M = 2.5$. The predicted Δt_c falls into the range of pulse intervals, as expected, within which the pattern of fringes experience a transition from more loosely spaced fringe cells to closely spaced small striations as the pulse interval decreases (compare Figs. 4c and 4d).

It also follows that as the pulse interval decreases, the contribution due to convection of large eddies to the optical phase shift becomes smaller, whereas that from smaller scale features increases relatively. Thus the smaller scales may be made visible by using appreciably smaller pulse intervals. In looking for the smaller scales, one finds that, on the differential interferograms taken with pulse intervals of 5 and 2 μs, highly stretched fringe cells appear to lean downstream with their legs attached to the wall (Figs. 4e and 4f). The portion of fringe cells near the wall is more inclined, whereas that in the outer part of the boundary layer is more vertical. This indicates an association of the inclination angle with the local shear stress. It is still not clear if these fringe cells are the images of hairpin vortices since their dimension appears larger than 100–$200\nu_w/u_\tau$ (probably because the pulse interval is not small enough to eliminate completely the influence of the large scale structures). It is plausible, however, to speculate that the two typical fringe patterns, i.e., the circular fringe cells (Fig. 4b) and the highly stretched fringe cells (Fig. 4e), reflect two identities of the outer-layer bulges, one as large-scale eddies and the other as an amalgamation of vertically stretched smaller scale features.

In general, the interferograms obtained at other Mach numbers and Reynolds numbers are similar to those presented in Fig. 4. In particular, it was found that similar cells tend to appear at shorter pulse intervals with increasing Mach number, showing that it is the distance that eddies travel between pulses that determines the overall pattern. No discernible differences could be seen between the fringe cells at $Re_\theta = 1.2 \times 10^4$ and 1.5×10^4 at $M = 1.8$. However, at $M = 2.5$ the patterns at $Re_\theta = 1.4 \times 10^4$ were less well defined than those at $Re_\theta = 2.2 \times 10^4$. Also the small spots surrounding the large-scale features noted in differential interferograms of long pulse intervals are absent at the lower Reynolds number (compare Fig. 4b with Fig. 5a), although they do occur in the patterns at $M = 3.6$ (Fig. 5b). It is likely that these tiny spot images observed are associated with the hairpin scale, since the dimension of these spot images coincides with that of the hairpin scale, which counts for one-twentieth to one-tenth of the boundary-layer thickness in these cases. More discussion and examples of photographs of these interference patterns can be found in Ref. 13.

In the present experiments, the absolute interferograms were taken with the image-plane interferometer since high spatial resolution of fringes is required for quantitative analysis. All of the differential interferograms, on the other hand, were taken with the diffuse-illumination interferometer. Interferograms produced with a diffused object beam contain three-dimensional information that can be seen by viewing the interferograms from different angles. This aids the study of turbulent structures. For example, by focusing the camera onto the tunnel floor it can be seen that there are about six cells lying across the spanwise section (Fig. 6), although they are not necessarily aligned in the same straight light path.

Numerical Postprocessing

If instantaneous density fields of compressible turbulent boundary layers are produced at successive instants by numerical simulations, interferograms can be generated by integrating the density changes across the flow. Unfortunately, due to the heavy demand on the computation and the memory capacity of computer work stations, most large-eddy simulations are carried out on very low speed flows without the presence of density variations. The database available for the present study was generated for a boundary layer developing over a flat plate at a freestream velocity of 9.6 m/s. Thus in the absence of density variations, it was decided to carry out the numerical postprocessing using either the pressure or a velocity component in place of density.

Simulated Database

The database used here was generated by Yang and Voke[14] at Surrey University. The computational domain has a dimension of $300 \times 30 \times 20$ mm. The $127 \times 56 \times 48$ computational mesh is distributed uniformly in the streamwise (x) and the spanwise (z) direction, but is stretched in the wall-normal direction (y) to resolve details of the flow very close to the wall. The inlet flow velocity is 9.6 m/s with a turbulent intensity of 6%. The transition to turbulence is found to occur at 60 mm from the leading edge of the flat plate. Because of the interest here in fully turbulent flows, the downstream half of the computational domain is chosen for the present analysis. In this region, the boundary-layer thickness (where $u = 0.99u_e$) grows gradually from 8 to 13 mm, and the Reynolds number based on the momentum thickness increases from 3×10^2 to 6×10^2.

The simulation was conducted in time steps of 10 μs and simulated flowfields at $t = 100$, 500, 1000, 2000, 5000, and 10,000 μs (relative to an arbitrary $t = 0$) were chosen for the present study. These intervals were chosen since they correspond to the same nondimensional time interval, $\Delta t u_\infty/\delta$, as used in the experiments at $M = 2.5$.

Numerical Interferograms

Initially absolute interferograms were formed from both the time-averaged and instantaneous longitudinal velocity fields (Figs. 7a and 7b). These interferograms show many of the features observed in the corresponding experimental interferograms. In particular, the instantaneous interferogram (Fig. 7b) shows the same ragged appearance as the experimental interferograms (see Fig. 1a), although the inclined interfaces penetrating the whole layer as observed in the experimental fringes are not easily identified.

The numerically generated differential interferograms are shown in Fig. 8. [Note that to give a clearer presentation of the fringe cells the fringes representing neutral phase shifts (not necessarily zero) are not shown on the plots.] On these interferograms, the cells of opposite signs in the radial gradient of phase shift are arranged in an alternative manner in most cases, with one upstream to the other and also one on the top of the other (see for example Fig. 8c). The size of these cells follows the growth of the boundary layer. The changes in the image pattern with the pulse interval basically agree with the observations on the experimental interferograms. In general, interferograms of a pulse interval $\Delta t \leq 2000\,\mu$s, during which flow features convect downstream by a distance smaller than 2δ, show

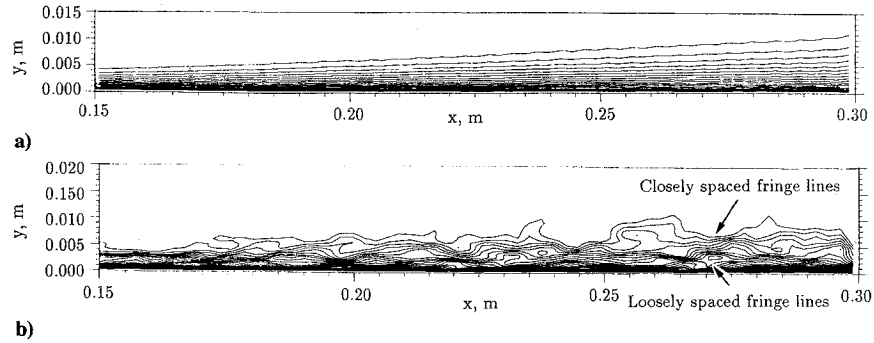

Fig. 7 Absolute interferograms generated with a) the time-averaged longitudinal velocity and b) the instantaneous longitudinal velocity at $t = 0$.

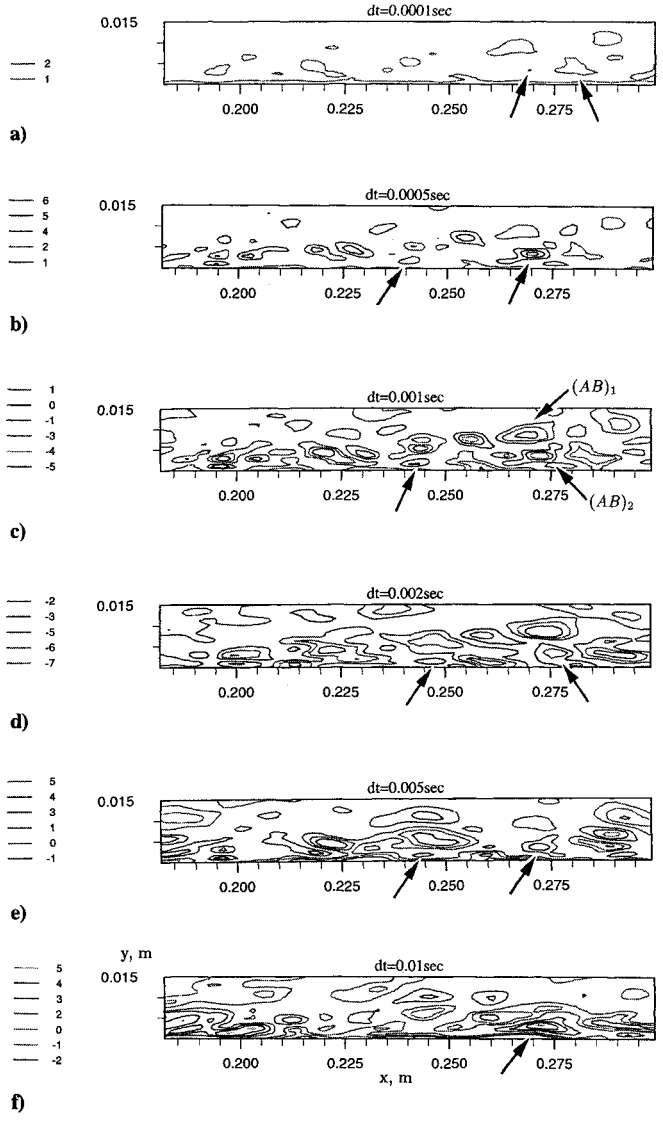

Fig. 8 Differential interferograms generated with the simulated longitudinal velocity fields.

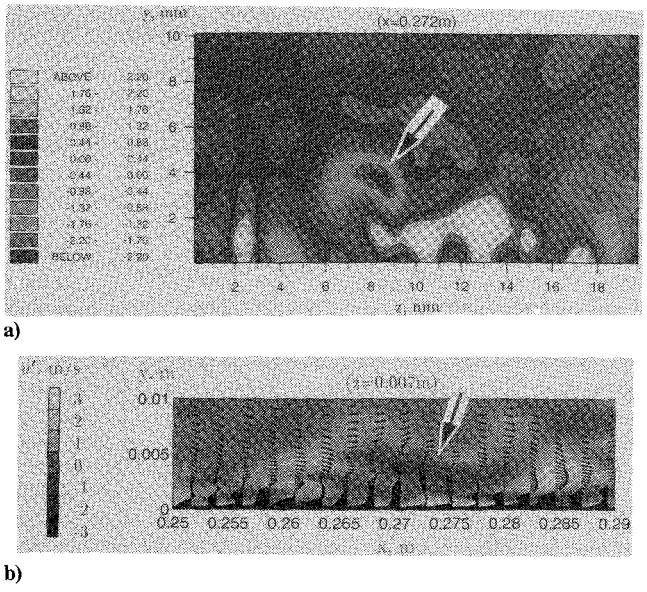

Fig. 9 Contours of fluctuating velocity: a) in the spanwise plane at x = 272 mm, and b) in the streamwise plane at z = 7 mm seen by an observer moving at $u = 0.8u_\infty$.

well-arranged fringe pattern along the whole length of the boundary layer since the images related to the same flow feature appear in the neighborhood of each other. One can also easily identify a number of fringe cells on each interferogram from their similarity in pattern. For example, the pair of cells with one on the top of the other at x = 240 and 270 mm (indicated by arrows) in Fig. 8b appears further downstream on Figs. 8c and 8d. The fringe pattern on interferograms of longer pulse intervals appears less regular since the resultant images are produced by superimposition of two flowfields that are less correlated. The images on the interferogram with a pulse interval of 10000 μs is least regular (see Fig. 8f), since the flow features have traveled a significant distance, which is about one-half of the flow domain shown on the plots. On the other hand, an image at a particular location on such an interferogram may be directly related to a flow feature appearing at that location at one of the time instants if there is no distinct feature existing there at the other instant.

Flowfield Survey

To understand the relation between the fringe patterns and the flow features in the boundary layer, regions that exhibit distinct fringe pattern were identified and a detailed survey was carried out of the flowfield of interest. As an example, the interferometric image in the neighborhood of x = 272 mm appears to be quite pronounced and shows distinct fringe cells on the differential interferograms (Fig. 8c) and an erratic fringe pattern on the absolute interferogram (Fig. 7b). This indicates that some distinct events occur along the spanwise section. The fluctuating longitudinal velocity contour in a y–z plane at x = 272 mm, Fig. 9a, reveals a strong circular feature (indicated by an arrow) with a velocity deficit relative to its surroundings. The velocity deficit at the center of the feature has a strength of 60% of the local mean velocity, which is strong enough to make itself seen. It is this circular feature that produces the loosely spaced fringes on the absolute interferogram (Fig. 7b) and the cell of negative gradient of phase shift at x = 272 mm in Fig. 8f. In particular, in a coordinate moving at a speed of $0.8u_\infty$ the low-speed feature is associated with a circular motion and exhibits a saddle point at its back (indicated by an arrow in Fig. 9b), in agreement with the picture of a turbulent bulge described by many other workers.[1–4] The high-speed patch around the top of this low-speed feature must be responsible for the closely spaced fringes on the top of the spreading region in Fig. 7b and the cell of positive gradient of phase shift at x = 272 mm in Fig. 8f.

Concluding Remarks

Double-pulse holographic interferometry has been used to visualize zero-pressure-gradient turbulent boundary layers over a flat plate at freestream Mach numbers of 1.8, 2.5, and 3.6. The interferograms obtained reveal clearly defined features in the flows. As a systematic study of organized structures using this method for the first time, efforts have been made to interpret the interferometric data, to extract information about these structures, and to study the effect of flow conditions on their characteristics. Quantitative data, such as the inclined angle of the large-scale outer-layer bulges, have been obtained, which are in agreement with data from research workers using different experimental techniques. The results also demonstrate the potential of interferometry in revealing smaller scale structures that are dynamically important.

Numerical interferograms have been generated with the database from a large-eddy simulation. Although the interferometric fringe patterns do not appear completely similar to those on the experimental interferograms due to the use of widely different flow parameters, distinct regular fringe patterns are observed, and they follow a similar change of pattern with pulse intervals as observed on the experimental interferograms. Furthermore, a study of these numerical fringe patterns in conjunction with surveys of the computed flowfield confirms the correspondence between interferometric fringe patterns and the distinct flow structures, thus aiding the interpretation of the experimental data. In particular the fact that a distinct interferometric fringe pattern at a given location can be related directly to a flow structure at that location goes some way to reducing concern regarding the possible adverse effects of integration along

the light path on the identification of turbulent structures. Further applications of this technique are encouraged.

In the present experiments, the range of Mach number and Reynolds number tested is limited by the capacity of the wind tunnel. It would be interesting to extend the flow conditions to a wider range of Mach number and Reynolds number so that their effects on the characteristics of organized structures can be further explored. Interferometry is also advantageous in the study of turbulence in complex turbulent flows such as shock and boundary-layer interactions where the application of most conventional measurement techniques is difficult. A better use of numerical postprocessing, however, still waits for the availability of databases for compressible flows at higher Reynolds numbers.

Acknowledgments

The first author would like to thank Churchill College, the British government, and the Zonta International Foundation for the financial support to her Ph.D. studies at Cambridge. Also, the authors wish to thank P. Voke and Z. Yang at Surrey University for their generosity in making accessible their large-eddy simulation database.

References

[1]Brown, G. L., and Thomas, A. S. W., "Large Structure in a Turbulent Boundary Layer," *Physics of Fluids*, Vol. 20, No. 10, 1977, pp. S243–252.

[2]Falco, R. E., "Coherent Motions in the Outer Region of Turbulent Boundary Layers," *Physics of Fluids*, Vol. 20, No. 10, 1977, pp. S124–132.

[3]Head, M. R., and Bandyopadhyay, P., "New Aspects of Turbulent Boundary-Layer Structure," *Journal of Fluid Mechanics*, Vol. 107, June 1981, pp. 297–338.

[4]Cantwell, B. J., "Organized Motion in Turbulent Flow," *Annual Review of Fluid Mechanics*, Vol. 13, 1981, pp. 457–515.

[5]Smith, M. W., "Flow Visualization in Supersonic Turbulent Boundary Layers," Ph.D. Dissertation, Dept. of Mechanical and Aerospace Engineering, Princeton Univ., New Haven, CT, 1989.

[6]Spina, E. F., Donovan, J. F., and Smits, A. J., "On the Structure of High-Reynolds-Number Supersonic Turbulent Boundary Layers," *Journal of Fluid Mechanics*, Vol. 222, Jan. 1991, pp. 293–327.

[7]Vest, C. M., *Holographic Interferometry*, Wiley, New York, 1979.

[8]Zhong, S., "An Interferometric Study of Organized Structures in Compressible Turbulent Flows," Ph.D. Dissertation, Engineering Dept., Univ. of Cambridge, Cambridge, England, UK, 1993.

[9]Squire, L. C., Bryanston-Cross, P. J., and Liu, X., "An Interferometric Study of the Shock Interaction at a Compression Corner," *Aeronautical Journal*, Vol. 95, No. 945, 1991, pp. 143–151.

[10]Marriott, P. G., "Compressible Turbulent Boundary layers with Discontinuous Air Transpiration," British Aeronautical Research Council, R & M 3780, Farnborough, UK, 1976.

[11]Jeromin, L. O. F., "An Experimental Investigation of the Compressible Turbulent Boundary Layer with Air Injection," British Aeronautical Research Council, R & M 3526, Farnborough, UK, 1968.

[12]Robinson, S. K., "Space-Time Correlation Measurements in a Compressible Turbulent Boundary Layer," AIAA Paper 86-1130, 1986.

[13]Zhong, S., and Squire, L. C., "Visualization of Organized Structures in Compressible Turbulent Flows by Holographic Interferometry," *Laser Techniques and Applications in Flow Mechanics*, edited by R. J. Adrian, W. Merzkirch, and J. H. Whitelaw, Springer–Verlag, Berlin, 1993, pp. 433–450.

[14]Yang, Z., and Voke, P. R., "Large-Eddy Simulation Studies of Bypass Transition," *Proceedings of 2nd International Symposium on Engineering Turbulence Modelling and Measurement*, Elsevier, Amsterdam, The Netherlands, 1993, pp. 603–611.